NANO LETTERS

Letter

pubs.acs.org/NanoLett

Kinetic Competition Model and Size-Dependent Phase Selection in 1-D Nanostructures

Yu Chen,[†] Yung-Chen Lin,[†] Chun-Wei Huang,[§] Chun-Wen Wang,[†,§] Lih-Juann Chen,[∥] Wen-Wei Wu,[§] and Yu Huang*[,†,‡]

[†]Department of Materials Science and Engineering, [‡]California NanoSystems Institute, University of California, Los Angeles, California 90095, United States

[§]Department of Materials Science and Engineering, National Chiao Tung University, Hsinchu 300, Taiwan

[∥]Department of Materials Science and Engineering, National Tsing Hua University, Hsinchu 300, Taiwan

Supporting Information

ABSTRACT: The first phase selection and the phase formation sequence between metal and silicon (Si) couples are indispensably significant to microelectronics. With increasing scaling of device dimension to nano regime, established thermodynamic and kinetic models in bulk and thin film fail to apply in 1-D nanostructures. Herein, we present an unique size-dependent first phase formation sequence in 1-D nanostructures, with Ni−Si as the model system. Interfacial-limited phase which forms the last in thin film, $NiSi_2$, appears as the dominant first phase at 300−800 °C due to the elimination of continuous grain boundaries in 1-D silicides. On the other hand, θ-Ni_2Si, the most competitive diffusion-limited phase takes over $NiSi_2$ and wins out as the first phase in small diameter nanowires at 800 °C. Kinetic parameters extracted from in situ transmission electron microscope studies and a modified kinetic growth competition model quantitatively explain this observation. An estimated critical diameter from the model agrees reasonably well with observations.

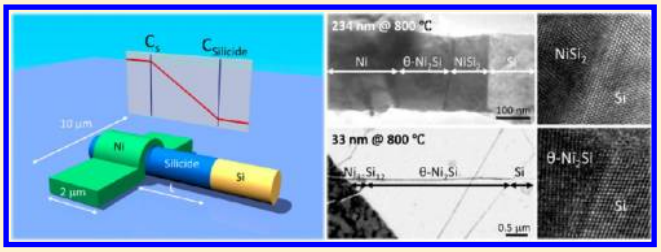

KEYWORDS: *Size dependent, kinetic competition, silicide, diffusion, silicon nanowire, phase sequence*

Size does matter. In low-dimensional structures, unique material properties and superior functions are available due to geometry effect. While the unique properties of nanostructured materials have been discovered and interrogated extensively in the past few decades,[1−7] fundamental material processes at this scale leave much to be desired for. For instance, nanoscale Si electronics have attracted much attention, wherein the contact engineering is of paramount importance leading to reliable and high device performance at this scale.[8−10] The thermodynamics and kinetics properties of metal silicide phases have been extensively studied in two-dimensional (2-D, thin film) and three-dimensional (3-D, bulk) structures for its significance in microelectronic applications.[11−13] There, the first formed silicide phases and the phase formation sequences were predicted by the effective heat of formation model and the transformation rate competition model.[14−16] Very interestingly, the phase transformation sequences in one-dimensional (1-D) Si nanostructures have been found to deviate from that of bulk and of thin film system, for which no consistent explanations are currently available.[17−22] Meanwhile, research has suggested that the atomic and molecular motions can be much altered in 1-D nanostructures.[6] Systematic investigation and understanding of the phase transformation process at nanoscale are hence prescribed to achieve predictable and reliable contacts for high-performance nanodevices.[23−25]

In this study, the phase transformation sequence of Ni−Si binary system in a Si nanwire (NW) template is extensively and systematically interrogated over a wide range of temperatures. Unique size-dependent first phase selection is found for the first time. Coexistence of multiple phases at initial stages confirms that the nonfirst phases are not limited by nucleation. Selection of first phases is governed by a kinetic growth competition. With kinetic parameters extracted from in situ transmission electron microscope (TEM) observations, a modified growth competition model is applied to predict the first phase sequence and yields a reasonable critical Si NW diameter. Beyond this critical diameter, the first phase can be switched from diffusion rate-limited phase (θ-Ni_2Si) to interfacial-limited phase ($NiSi_2$) at 800 °C.

Here, all samples are prepared on Si nitride TEM membranes with a previously reported approach.[9,10] Si (111) NW are synthesized from vapor−liquid−solid method with Au as catalyst to control the diameter of Si NWs. Typical Si NWs are single crystal with diameter of 20−234 nm and length of 15−20 μm. To make a Si/silicide heterostructure, Si NWs are first dispersed on top of Si nitride membranes and partially

Received: March 13, 2012
Revised: April 16, 2012
Published: April 30, 2012

covered by Ni pads patterned by e-beam lithography. In a vacuum order of 10^{-8} Torr, 70 nm thick, 2 μm width Ni pads are deposited by e-beam evaporator. To provide good contacts between Ni and Si, buffered oxide etchant (BOE, commercial HF buffered solution) is used to remove native oxides before the depositions of Ni films. Samples are loaded into e-beam metal deposition chamber right after the BOE treatment and then annealed at 300−800 °C for different durations in in situ TEM (JEOL CX100 TEM and JEOL JEM-2000 V equipped with Gatan heating holder). High-resolution image of epitaxial relation and characterizations of silicide are performed with FEI Titan-300 KV.

During the annealing process, Ni diffuses into Si NW and forms Ni silicides. Multiple silicide phases are identified growing from underneath of Ni pads into the Si NW template (Figure 1a). Cubic $NiSi_2$ (space group 225, $Fm\bar{3}m$, a = 5.416 Å),

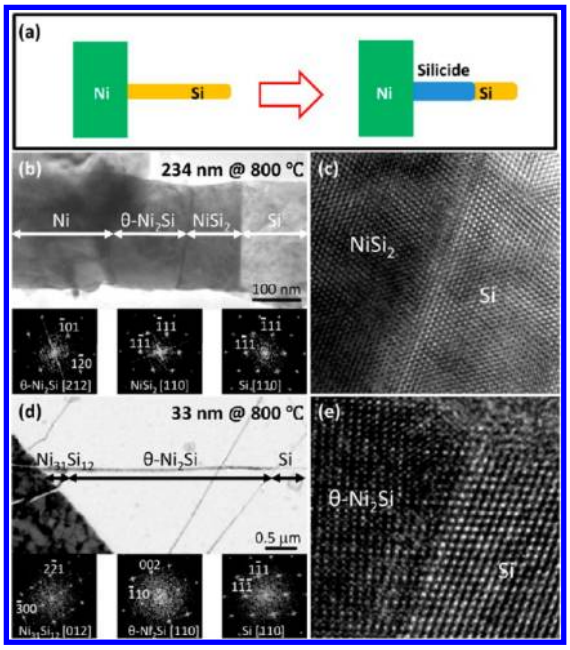

Figure 1. Size-dependent first phase selection at 800 °C. (a) Schematics of typical heterostructure. (b,c) Silicides formed in a 234 nm Si NW grown at 800 °C for 30 s. (b) Image and FFT patterns of θ-Ni_2Si, $NiSi_2$ and Si. (c) Epitaxial interface between $NiSi_2$ and Si. (d,e) Silicides formed in a 33 nm Si NW grown at 800 °C for 30 s. (d) Image and FFT patterns of $Ni_{31}Si_{12}$, θ-Ni_2Si and Si. (e) Epitaxial interface between θ-Ni_2Si and Si.

hexagonal θ-Ni_2Si (space group 194, $P6_3/mmc$, a = 3.805 Å, and c = 4.890 Å), orthogonal δ-Ni_2Si (space group 62, $Pnma$, a = 4.990 Å, b = 3.720 Å, and c = 7.030 Å) and hexagonal $Ni_{31}Si_{12}$ (space group 150, $P321$, a = 6.671 Å, and c = 12.288 Å) are confirmed from high-resolution images and fast Fourier transform (FFT) patterns at two different zone axis (Figure S1, Supporting Information). The atomic structures of $NiSi_2$, δ-Ni_2Si, and $Ni_{31}Si_{12}$ are close to previously reported silicides NWs grown with chemical vapor deposition where hexagonal $Ni_{31}Si_{12}$ is different from monoclinic β_3-Ni_3Si.[26−29] According to phase diagram, hexagonal θ-Ni_2Si which is thermodynamically stable only above 816 °C with composition range from Ni:Si = 1.564 to 1.941 is different from orthogonal δ-Ni_2Si (line product, stable down to room temperature).[30] Since the growth time of silicides in Si NW template is short and no higher temperature postannealing is applied, metastable θ-Ni_2Si can remain as the first phase which was consistent with the observation in [112] Si NW template.[19]

Through identification of silicide phases with TEM at 800 °C, a significant size-dependent first phase selection is observed, i.e., while $NiSi_2$ remains as the first phase in a Si NW larger than 150 nm (Figure 1b,c), θ-Ni_2Si takes over $NiSi_2$ and becomes the first phase in a Si NW with diameter smaller than 70 nm (Figure 1d,e). However, it is observed that at lower temperatures, 300−650 °C, $NiSi_2$ emerges as the first phase in all examined Si NW templates with a diameter of 27−213 nm (Figure 2 and Figure S2, Supporting Information). Epitaxial

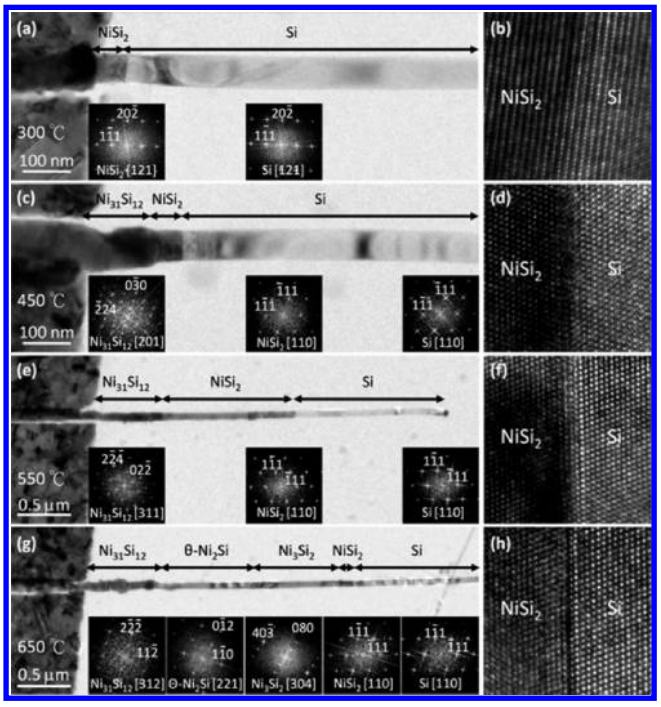

Figure 2. TEM images of silicides formation sequence and silicide/Si interface in ∼50 nm Si NW templates annealed at various temperatures. $NiSi_2$ emerges as the first phase in all cases from 300 to 650 °C. (a,b) 300 °C for 30 min; (c,d) 450 °C for 30 s; (e,f) 550 °C for 30 s; and (g,h) 650 °C for 30s. There is no silicide grow out from Ni pad below 300 °C within 1 h. All $NiSi_2$/Si interface keeps epitaxial relation of $NiSi_2[110]//Si[110]$ and $NiSi_2(-111)//Si(-111)$.

relations $NiSi_2[110]//Si[110]$ and $NiSi_2(-111)//Si(-111)$ are found between $NiSi_2$ and Si (Figure 2b,d,f,h). With systematic studies, we rule out Si/silicide interfacial strained energies (at epitaxial interfaces) and effective heat of formation difference among phases as key contributors (Supporting Information for detailed discussion) but confirm that the kinetic growth competition determines the first phase formation in Si NW templates.

In our models, several phases conucleate at the initial stage, and the phase with fastest growth rate wins out and grows as the first phase. In order to confirm the existence of multiple phases present at the initial stage of nucleation and growth under Ni pads and for the convenience of observation, we adopt an analogous structure as shown in Figure 3a. A Si NW is fully covered on one side with 10 nm evaporated Ni and subject to annealing at 800 °C for 5 s. With limited Ni supply and annealing time, the formed silicides are captured at the initial stage and the short annealing (5 s) also prevents the existing silicides from transforming into other phases with the

dx.doi.org/10.1021/nl300990q | Nano Lett. 2012, 12, 3115−3120

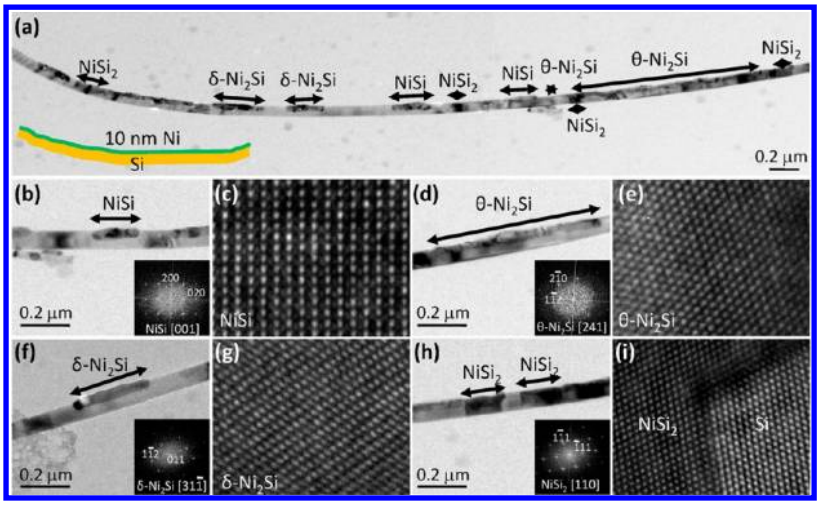

Figure 3. Coexistence of multiple phases at the initial growth stage (with native oxide between Ni/Si NW). (a) Low-magnification TEM image of silicides grown in Si NW template. Si NW is covered by 10 nm Ni at upper side and annealed for 5 s at 800 °C; (inset) schematic of 10 nm Ni on Si NW. (b,c) Zoom in TEM, atomic resolution images, and corresponding FFT pattern of NiSi. (d,e) Zoom in TEM, atomic resolution images, and corresponding FFT pattern of θ-Ni_2Si. (f,g) Zoom in TEM, atomic resolution images, and corresponding FFT pattern of δ-Ni_2Si. (h,i) Zoom in TEM, atomic resolution images, and corresponding FFT pattern of $NiSi_2$.

remaining Ni or Si sources. High-resolution TEM (HRTEM) images of each phase and corresponding FFT patterns are used to identify the observed silicides (Figure 3b–i and Figure S3b–g, Supporting Information). As shown in Figure S3, Supporting Information, θ-Ni_2Si, $NiSi_2$, and δ-Ni_2Si are coexisting as small domains contacting each other without clear boundaries or specific sequence. It indicates that nucleation does not limit the appearance of nonfirst phase silicides. To further clarify, if these phases nucleate independently or are transformed from previous generated silicide with remaining Ni or Si source, a similar structure but with native oxide (<1 nm thick) between Ni and Si NW template (Figure 3) is examined. In this structure, Ni atoms penetrate through thin shell or local weak points to form separate silicide domains that do not contact with each other. Again, θ-Ni_2Si, $NiSi_2$, δ-Ni_2Si, and NiSi are found coexisting between Ni and Si separately. Diffusion rate-limited phases, θ-Ni_2Si, δ-Ni_2Si, and NiSi, form small islands close to the Ni source, and interfacial-limited $NiSi_2$ forms a single crystalline section exhibiting {111} facets and has an epitaxial relation of $NiSi_2[110]//Si[110]$, $NiSi_2(-111)//Si(-111)$ with Si. NiSi was only observed in Figure 3 but did not appear in Figure S3, Supporting Information, where the native oxide is removed and all domains make contact with each other. It might be attributed to the slower growth rate of NiSi which results in its consumption by the faster growing phases in contact. Coexistence of Ni silicide phases in Figure 3a and Figure S3, Supporting Information, confirms independent nucleation of multiples phases from Ni/Si reaction couple at the initial stage. The observed first phases, $NiSi_2$ and θ-Ni_2Si, in 1-D Si NW template are selected through growth competitions among different phases.

The predominance of $NiSi_2$ as the first phase at lower temperatures, and the appearance of θ-Ni_2Si and $NiSi_2$ at higher temperatures can be explained by a modified kinetic growth competition mechanism in 1-D nanostructures. Comparing to 2- and 3-D structures, the small size of NWs eliminates the continuous grain boundary in silicides (axial direction), which is a fast path of Ni diffusion.[31] Thus, in 1-D structures, the growth rate of the diffusion-limited phases, such as δ-Ni_2Si (conventional first phase in thin film), decreases significantly, which renders the growth of interfacial-limited phase, i.e., $NiSi_2$, competitive. Among the diffusion-limited phases, θ-Ni_2Si gives the fastest Ni diffusion rate,[32] which explains the observation that only the θ-Ni_2Si phase appears as the competitive phase against $NiSi_2$ at high temperatures.

In situ TEM studies are then employed to confirm growth mechanisms and to extract kinetic parameters. Within a single crystal lattice Si NW, in situ TEM provides high temporal resolution observation of the silicide growth front, from which the accurate kinetic data, such as the diffusivity, the reaction rate constant, and the activation barriers of the silicides, can be readily extracted to quantitatively explain the observed size-dependent first phase selection at 800 °C (Figure 4). In addition, due to single crystal nature of Si NW and the elimination of grain boundaries in this template, the kinetic data will represent the intrinsic lattice properties, which may be compared to the bulk data to differentiate the contributions from various components, e.g., lattice diffusion vs grain boundary diffusion.

We define L as the total length of silicides from Ni source to the silicide/Si interface at time t (Figure S4, Supporting Information) and plot the $L-t$ diagram with data captured from in situ TEM observations. The growth length L of θ-Ni_2Si shows a parabolic relation with growth time t, which indicating that the rate-limiting step is Ni diffusion to silicide/Si interface (Figure 4a). Interestingly, $NiSi_2$ exhibits clearly two different stages: a linear growth (interfacial-limited) during the first stage of growth followed by a parabolic growth behavior (diffusion-limited), indicating a linear–parabolic transition (Figure 4b).[33] The in situ studies show transition lengths from 341 to 1581 nm at 500 to 650 °C. There is no obvious transition at 450 °C due to the short growth length during the observation duration. In our structure, native SiO_2 at Si NW surface is removed by BOE before the deposition of Ni source, hence we do not expect the rate-limiting step coming from Ni and diffusing through native oxide at the Ni/silicide interface.[34] The interfacial-limited behavior therefore is a result of the growth rate-limited step at the $NiSi_2$/Si interface and not at Ni/silicide interface.

In the 2-D system, $NiSi_2$ only appears at higher temperatures (>750 °C) and usually as the last phase following the formation

dx.doi.org/10.1021/nl300990q | Nano Lett. 2012, 12, 3115–3120

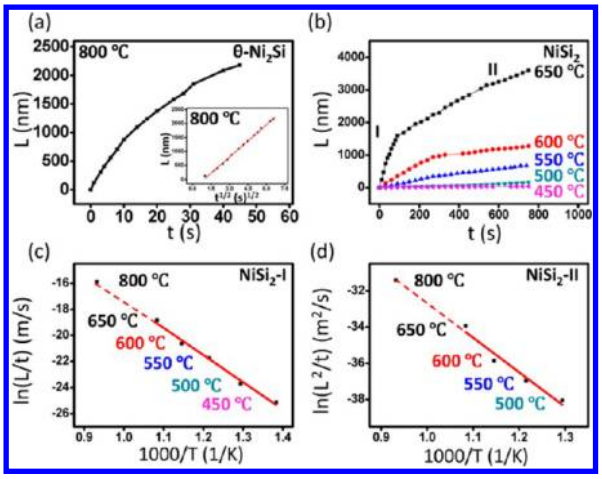

Figure 4. Growth behaviors of θ-Ni_2Si and $NiSi_2$ in Si NW templates with diameter of ~70 nm from 450 to 800 °C observed with in situ TEM. (a) Growth length vs time of θ-Ni_2Si at 800 °C; (inset) growth length vs square root of time of θ-Ni_2Si at 800 °C to confirm nature of parabolic growth. (b) Growth length of $NiSi_2$ vs time from 450 to 650 °C. Linear to parabolic transitions are observed at 341−1581 nm at 500−650 °C, respectively. (c) Arrhenius' plot of reaction rate of $NiSi_2$ front with activation barrier of 1.792 ± 0.101 eV/atom from the linear growth region ($NiSi_2$-I). (d) Arrhenius' plot of Ni diffusion in $NiSi_2$ with activation barrier of 1.641 ± 0.237 eV/atom, from parabolic region ($NiSi_2$-II).

of NiSi. This has hindered the examination of the kinetic behaviors of $NiSi_2$ formation over a wide range of temperatures and larger distances as well as masked the $NiSi_2$ formation behavior from the intrinsic Ni−Si couple. As a result, to our best knowledge, the kinetic data for $NiSi_2$ are very limited from bulk studies. The emergence of the $NiSi_2$ as the first phase in Si NW template and its persistent existence as the first phase over a wide range of temperatures (~ 300−800 °C) and over long distance (hundreds of nanometers to micrometers) have allowed us to closely interrogate its kinetic behavior for the first time. We clearly captured the two-stage transition of $NiSi_2$ in a single crystal Si lattice, which has allowed the first time derivation of the reaction rate constant K_R of $NiSi_2$ from regime $NiSi_2$-I (Figure 4c) and the diffusivity D during the later parabolic diffusion-limited growth stage, $NiSi_2$-II (Figure 4d).

If we simplify the kinetic model by assuming a steady-state reached, i.e., the Ni diffusion flux through silicides is equal to the flux consumed for interface reaction, then we can obtain the relation of silicide grown length L and time t (Figure S4, Supporting Information for derivation and data extraction):

$$L = \frac{A}{2}\left(\sqrt{1 + \frac{(t+\tau)}{A^2/4B}} - 1\right) \quad (1)$$

$$A = \frac{2D}{K_R} \quad (2)$$

$$B = \frac{2DMC_s}{b\rho} \quad (3)$$

$$\tau = \frac{L_0^2 + AL_0}{B} \quad (4)$$

Here, K_R is the reaction rate constant at silicide/Si interface, D is diffusivity of Ni through silicide, L_0 is the total length of silicide at $t = t_0$, which is 0 in our case, b is number of Ni atoms in silicide formula (2 for θ-Ni_2Si and 1 for $NiSi_2$), M is the atomic weight of silicides, ρ is the density of silicides, and C_s is the Ni concentration per unit volume at the Ni/silicide interface.

For a short growth time period, $t \ll A^2/4B$, eq 1, can be approximated by

$$L = \frac{A}{2}\left(1 + \frac{1}{2}\left(\frac{t}{A^2/4B}\right) - 1\right) = \frac{Bt}{A} = \frac{MC_sK_Rt}{b\rho} \quad (5)$$

For a long growth time period, $t \gg A^2/4B$, eq 1, can be approximated by

$$L = \frac{A}{2}\sqrt{\frac{t}{A^2/4B}} = \sqrt{Bt} = \sqrt{\frac{2DMC_st}{b\rho}} \quad (6)$$

Since C_s is the Ni concentration at Ni/silicide interface where Ni is always abundant, we assume C_s equals to the Ni mole concentration in Ni source (C_s = 0.1517 mol/cm^3). From eqs 5 and 6, we can extract K_R and D values from the $L-t$ relations, as shown in Table 1, and the corresponding activation energies.

Table 1. Kinetic Parameters of Ni Silicides Extracted from in Situ TEM Observations[a]

	temperature °C	K (m/s)	D (m^2/s)	D_o (m^2/s)
$NiSi_2$	450	1.23×10^{-11}		
	500	5.07×10^{-11}	2.99×10^{-16}	
	550	3.58×10^{-10}	8.86×10^{-16}	
	600	1.09×10^{-9}	2.67×10^{-16}	1.20×10^{-6}
	650	6.57×10^{-9}	1.85×10^{-15}	
	800	$\mathbf{1.20 \times 10^{-7}}$	$\mathbf{2.33 \times 10^{-14}}$	
θ-Ni_2Si	800		3.65×10^{-14}	

[a] K is the reaction rate constant at silicide/Si interface; D is the Ni diffusivity in silicides; and D_0 is the maximum diffusivity of Ni in $NiSi_2$. Numbers in bold represent data obtained by linear extrapolation to 800 °C.

Assuming both the interfacial reaction barrier and the diffusion barrier of Ni in $NiSi_2$ are the same, then K_R and D values of $NiSi_2$ at 800 °C (as shown in bold in Table 1) are able to be linear extrapolated from the data of 450−650 °C.

The activation barrier for Ni diffusing through $NiSi_2$ is 1.641 ± 0.237 eV/atom during the diffusion-limited stage ($NiSi_2$-II, Figure 4d), and the activation barrier of $NiSi_2$ interface reaction is 1.792 ± 0.101 eV/atom at the earlier growth stage ($NiSi_2$-I, Figure 4c). There is no available diffusivity and activation barrier data from thin film studies to describe the Ni diffusion in the $NiSi_2$, as $NiSi_2$ usually appears as the last phase in crystalline Si. However, the derived 1.641 ± 0.237 eV/atom activation energy for Ni diffusion in $NiSi_2$ is very close to the 1.65 ± 0.20 eV/atom barrier height reported in amorphous Si, where diffusion-limited growth of $NiSi_2$ was observed.[35] This indicates the grain boundary contribution is not significant in Ni diffusion in $NiSi_2$, otherwise a much lower diffusivity and higher barrier should be found in single crystal silicide section (in Si NW). Comparing the activation energies of $NiSi_2$ to that of δ-Ni_2Si, which is the first formed phase in a thin film and bulk system, elimination of continuous grain boundary (axial direction) in 1-D silicide structure raises the growth activation barrier of δ-Ni_2Si from 1.30 to 1.70 eV/atom (grain boundary dominated diffusion) to 2.48 eV/atom (lattice diffusion),[31] which is higher than both the activation barrier of $NiSi_2$ interface reaction (1.792 ± 0.101 eV/atom) and the activation energy for Ni diffusion in $NiSi_2$ (1.641 ± 0.237 eV/atom).

dx.doi.org/10.1021/nl300990q | Nano Lett. 2012, 12, 3115−3120

This data are consistent with our observation that the first phase is flipped from δ-Ni_2Si (in the thin film system) to $NiSi_2$ (in Si NWs) and confirms the hypothesis that elimination of grain boundaries renders $NiSi_2$ more competitive in 1-D structures.

With extracted parameters, we are able to compare the transformation rate of $NiSi_2$ and θ-Ni_2Si and to understand their growth competition in 1-D Si NW templates. Here we replace L in eqs 5 and 6 with "d" to represent the diffusion path length at radial direction, assuming the kinetic parameters are similar in radial and axial directions. According to D and K_R in Table 1, the average transformation rates of θ-Ni_2Si and $NiSi_2$ (70 nm far from Ni source) are 1.458 and 0.438 μm/s, respectively, at 800 °C. In this region, the average growth rate of θ-Ni_2Si is 3.3 times that of the $NiSi_2$, consistent with our observation of θ-Ni_2Si appearing as the winning first phase. However, with increasing diffusion path (d), the growth rate of diffusion-limited θ-Ni_2Si will decelerate, while the growth rate of the interfacial-limited $NiSi_2$ remains constant and will eventually catch up then take over θ-Ni_2Si. By setting eqs 5 = 6 (when both phases grow the same distance at a given time), we arrive at critical values of d_c = 234 nm, beyond which the switch from θ-Ni_2Si to $NiSi_2$ is possible.

In our Si NW system, $NiSi_2$ was found as first phase in Si NWs with diameter larger than 150 nm, which is very close to the estimated value. The difference may arise from the assumptions of simultaneous nucleation of $NiSi_2$ and θ-Ni_2Si at t_0. In reality the nucleation of $NiSi_2$ may initiate earlier than θ-Ni_2Si for the following reasons: first of all, it is easier to reach Ni oversaturation to form $NiSi_2$ than to θ-Ni_2Si due to difference of compositions, i.e., 33.3% Ni in $NiSi_2$ and 66.7% in θ-Ni_2Si. Second, $NiSi_2$ is more stable than θ-Ni_2Si at lower temperatures, which may give $NiSi_2$ a jump start during the 30 s ramping time in our experiment. Indeed, a control sample annealed at 450 °C for 30 s demonstrates the growth of 210 nm long $NiSi_2$ from the Ni source (Figure 2c,d). Thus the inevitable ramping stage gives $NiSi_2$ the added edge in the competition to win out as the first phase in Si NWs with smaller diameter than the predicted critical value.

We have demonstrated that the size-dependent phase selection in Si NW templates can be understood with a modified kinetic competition model in 1-D nanostructures. Coexistence of multiple phases at initial stage confirms nucleation does not limit the appearance of nonfirst phases. Our studies suggest diffusion-limited δ-Ni_2Si (conventional first phase in thin film) is suppressed in the Si NW due to the elimination of grain boundary diffusion, instead, interfacial-limited $NiSi_2$ appears as the dominant first phase in Si NWs. In the 1-D nanotemplate, linear–parabolic transition was observed for $NiSi_2$ in crystalline Si lattice, which enables the first time extraction of the activation energies for the Ni diffusion in $NiSi_2$ lattice and the interface reaction at Si/$NiSi_2$. In specific, similar value of activation barrier and diffusivity of Ni diffusion in single crystal $NiSi_2$ (in Si NW) and in polycrystalline $NiSi_2$ suggests grain boundary diffusion is not a significant contribution. The studies also demonstrate that the activation barriers of $NiSi_2$ are lower than that of δ-Ni_2Si for lattice diffusion but higher than the diffusion barrier of δ-Ni_2Si through grain boundaries, confirming that the elimination of grain boundaries renders $NiSi_2$ more competitive, leading to its replacement of δ-Ni_2Si as the first phase in 1-D Si NW. The extracted parameters are then used to explain the kinetic competition which leads to the size-dependent first phase selection observed at 800 °C. With the understanding of kinetic growth competition at nanoscale, this model may be extended to predict phase formation sequence in other silicides, germanides, and metal alloy systems. This study demonstrated the potential for reliable and predictable phase formation for high-performance nanodevices through the fundamental understanding of the kinetics of material behaviors at nanoscale.

■ ASSOCIATED CONTENT

Ⓢ Supporting Information

Supporting text rules out interfacial strained energy and effective heat of formation as key contributors to first phase selections. Figure S1 shows FFT patterns of $NiSi_2$ and θ-Ni_2Si to identify the first phases. Figure S2 shows $NiSi_2$ emerges as the first phase in 27–213 nm Si NW at 550 °C. Figure S3 shows coexistences of silicides at initial growth stage (without native oxide). Figure S4 derives eqs 1–4 with a steady-state kinetic model. This material is available free of charge via the Internet at http://pubs.acs.org.

■ AUTHOR INFORMATION

Corresponding Author

*E-mail: yhuang@seas.ucla.edu

Notes

The authors declare no competing financial interest.

■ ACKNOWLEDGMENTS

The authors thank Prof. King-Ning Tu for helpful discussions and comments. Y.H. acknowledges support from the Center on Functional Engineered Nano Architectonics (FENA), Henry Samueli School of Engineering and Applied Science Fellowship, and Sloan Research Fellowship. We thank Electron Imaging Center of Nanomachines at CNSI and Dr. Sergey Prikhodko for the TEM support and discussions.

■ REFERENCES

(1) McFadden, S. X.; Mishra, R. S.; Valiev, R. Z.; Zhilyaev, A. P.; Mukherjee, A. K. *Nature* **1999**, *398*, 684–686.
(2) Wang, Z. L. *Mater. Sci. Eng., R* **2009**, *64*, 33–71.
(3) Hochbaum, A. I.; Chen, R.; Delgado, R. D.; Liang, W.; Garnett, E. C.; Najarian, M.; Majumdar, A.; Yang, P. *Nature* **2008**, *451*, 163–168.
(4) Leonard, F.; Talin, A. A. *Phys. Rev. Lett.* **2006**, *97*, 026804.
(5) Norris, D. J.; Bawendi, M. G. *Phys. Rev. B* **1996**, *53*, 16338–16346.
(6) Holmberg, V. C.; Panthani, M. G.; Korgel, B. A. *Science* **2009**, *326*, 405–407.
(7) Landman, U.; Barnett, R. N.; Scherbakov, A. G.; Avouris, P. *Phys. Rev. Lett.* **2000**, *85*, 1958–1961.
(8) Wu, Y.; Xiang, J.; Yang, C.; Lu, W.; Lieber, C. M. *Nature* **2004**, *430*, 61–65.
(9) Lin, Y. C.; Lu, K. C.; Wu, W. W.; Bai, J.; Chen, L. J.; Tu, K. N.; Huang, Y. *Nano Lett.* **2008**, *8*, 913–918.
(10) Lin, Y. C.; Chen, Y.; Shaios, A.; Huang, Y. *Nano Lett.* **2010**, *10*, 2281–2287.
(11) Chen, L. J. *JOM* **2005**, *57* (9), 24–30.
(12) Chen, L. J. *Mater. Sci. Eng., R* **2000**, *29*, 115–152.
(13) Murarka, S. P. *Intermetallics* **1995**, *3*, 173–186.
(14) Pretorius, R.; Marais, T. K.; Theron, C. C. *Mater. Sci. Eng., R* **1993**, *10*, 1–83.
(15) Gosele, U.; Tu, K. N. *J. Appl. Phys.* **1982**, *53*, 3252–3260.
(16) Wohlert, S.; Bormann, R. *J. Appl. Phys.* **1999**, *85*, 825–832.
(17) Lu, K. C.; Wu, W. W.; Wu, H. W.; Tanner, C. M.; Chang, J. P.; Chen, L. J.; Tu, K. N. *Nano Lett.* **2007**, *7*, 2389–2394.
(18) Weber, W. M.; Geelhaar, L.; Unger, E.; Cheze, C.; Kreupl, F.; Riechert, H.; Lugli, P. *Phys. Status Solidi B* **2007**, *244*, 4170–4175.
(19) Dellas, N. S.; Liu, B. Z.; Eichfeld, S. M.; Eichfeld, C. M.; Mayer, T. S.; Mohney, S. E. *J. Appl. Phys.* **2009**, *105*, 094309.

(20) Chou, Y. C.; Wu, W. W.; Lee, C. Y.; Liu, C. Y.; Chen, L. J.; Tu, K. N *J. Phys. Chem. C* **2011**, *115*, 397−401.
(21) Lin, Y. C.; Chen, Y.; Xu, D.; Huang, Y. *Nano Lett.* **2010**, *10*, 4721−4726.
(22) Ogata, K.; Sutter, E.; Zhu, X.; Hofmann, S. *Nanotechnology* **2011**, *22*, 365305.
(23) Léonard, F.; Talin, A. A. *Nat. Nanotechnol.* **2011**, *6*, 773−783.
(24) Lin, Y. C.; Chen, Y.; Huang, Y. *Nanoscale* **2012**, *4* (5), 1412−1421.
(25) Schmitt, A. L.; Higgins, J. M.; Szczech, J. R.; Jin, S. *J. Mater. Chem.* **2010**, *20* (2), 223−235.
(26) Lee, C. Y.; Lu, M. P.; Liao, K. F.; Lee, W. F.; Huang, C. T.; Chen, S. Y.; Chen, L. J. *J. Phys. Chem. C* **2009**, *113* (6), 2286−2289.
(27) Song, Y.; Schmitt, A. L.; Jin, S. *Nano Lett.* **2007**, *7* (4), 965−969.
(28) Lee, C. Y.; Lu, M. P.; Liao, K. F.; Wu, W. W.; Chen, L. J. *Appl. Phys. Lett.* **2008**, *93* (11), 113109.
(29) Song, Y. P.; Jin, S. *Appl. Phys. Lett.* **2007**, *90* (17), 173122.
(30) Miettinen, J. *Calphad* **2005**, *29* (3), 212−221.
(31) Colgan, E. G.; d'Heurle, F. M. *J. Appl. Phys.* **1996**, *79*, 4087−4095.
(32) Gulpen, J. H.; Kodentsov, A. A.; Vanloo, F. J. J. *Z. Metallkd* **1995**, *86*, 530−539.
(33) Gas, P.; d'Heurle, F. M. *Appl. Surf. Sci.* **1993**, *73*, 153−161.
(34) Yaish, Y. E.; Katsman, A.; Cohen, G. M.; Beregovsky, M. *J. Appl. Phys.* **2011**, *109*, 094303.
(35) Lien, C. D.; Nicolet, M. A.; Lau, S. S. *Phys. Status Solidi A* **1984**, *81*, 123−128.